Journal of Engineering and Sustainable Development
www.jeasd.org
Vol. 21, No.01, January 2017
ISSN 2520-0917

FINITE ELEMENT ANALYSIS OF PORCELANITE LIGHTWEIGHT AGGREGATE REINFORCED CONCRETE DEEP BEAMS STRENGTHENED BY EXTERNALLY BONDED CARBON FIBER STRIPS

Dr. Kaiss F. Sarsam[1], Dr. Nabeel A.M. Al-Bayati [2], *Ahlam S. Mohammed [3]

1) Professor., Department of Building and Construction Engineering, University of Technology, Baghdad, Iraq
2) Professor, Department of Building and Construction Engineering, University of Technology, Baghdad, Iraq
3) Ph.D postgraduate candidate in structural engineering, Department of Building and Construction Engineering, University of Technology, Baghdad, Iraq

Abstract: A nonlinear finite element analysis carried out to investigate the behavior of a simply supported reinforced concrete deep beams to study their shear behavior after being strengthened by externally bonded carbon fiber composites materials (CFRP). Seven identical porcelanite lightweight aggregate concrete deep beams were analyzed numerically by using ANSYS computer program, two of them were unstrenghtened to serve as reference beams while the remaining five were strengthened using carbon fiber strips in different orientations (vertical, horizontal and inclined) and different number of layers (one and two layers). The locally available natural porcelanite aggregate (from western region of Iraq) was used to produce a structural lightweight aggregate concrete. Two different values of the shear span to depth ratio were adopted. The finite element analysis covers load-midspan deflection behavior, first shear crack and ultimate loads, and the crack pattern of the tested deep beams. Good agreement is obtained with available results which indicate the efficiency of the finite element method used to model the problem.

Keywords**:** *deep beams, CFRP strengthening, lightweight concrete, shear failure, nonlinear analysis, finite element analysis.*

التحليل اللاخطي باستخدام طريقة العناصر المحددة لعتبات خرسانة البورسيلانايت خفيفة الوزن المسلحة العميقة والمقواة خارجيا بشرائح الياف الكاربون

الخلاصة: يتضمن هذا البحث التحليل اللاخطي للعتبات الخرسانية المسلحة بسيطة الاسناد لبحث امكانية زيادة قابلية تحملها لاجهاد القص بعد ان يتم تقويتها خارجيا باستعمال شرائح الياف الكاربون. تم في هذا االبحث تحليل سبع عتبات عميقة خفيفة الوزن متماثلة و مصنوعة من حجر البورسيلانايت باستخدام برنامج ال (ANSYS) . اثنان من هذه العتبات كانتا غير مقواة خارجيا بالياف الكاربون وذلك لاستخدامها لاغراض المقارنه مع العتبات الخمس المتبقية المقواة خارجيا بالياف الكاربون بوضعيات مختلفة (افقي، شاقولي ومائل) وبعدد طبقات مختلف من الياف الكاربون (طبقة واحدة او طبقتين). تم استخدام صخور البورسيلانايت (المتوفرة في المنطقة الغربية للعراق) في انتاج خرسانه خفيفة الوزن ذات مقاومه مقبوله انشائيا. تم استعمال قيمتين مختلفتين لنسبة فضاء القص الى العمق الفعال في تحليل العتبات المسلحة العميقة. شمل التحليل اللاخطي دراسة تغير الهطول لمنتصف العتبة مع تغير مقدار الحمل المسلط على العتبات، ومقدار الحمل المسبب لاول شق قص وتثبيت مقدار الحمل الاقصى للعتبات، وكذلك دراسة تغير شكل الشقوق المتكونه عند التحميل

*Corresponding Author Ahlamsader@yahoo.com

ودراسة ثاثير الياف الكاربون على هذه الشقوق. تم تقييم دقة النتائج النتائج المستحصله من خلال المقارنة مع النتائج التجريبية المتاحة والتي تم اجرائها في سياق هذه الدراسة. وتم الحصول على توافق جيد ومقبول مع النتائج العملية المتاحة والتي تشير أيضا الى كفاءة طريقة العناصر المحددة المستخدمة في تمثيل العتبات قيد البحث.

1. Introduction

Deep beam are defined as a structural element which has a large depth to span ratio such that a considerable amount of the applied loads are transferred to beams' supports by a compression thrust joining the supports and the applied load points. According to ACI 318M-14[1], deep beams should satisfy one of the following conditions (Fig. 1).

1) Clear span (measured face to face of supports) does not surpass four times the overall depth of the deep beam (h), or $l_n / h \leq 4$

2) Concentrated loads are applied within twice the depth of the deep beam, or $a < 2h$

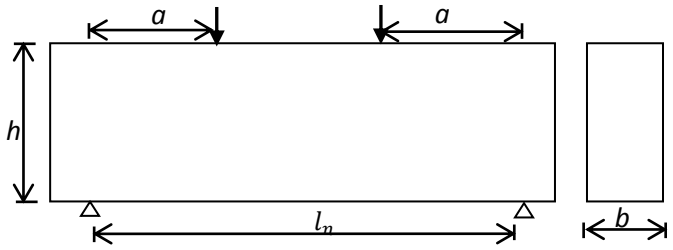

Figure 1. Deep beam dimensions

Deep beams are found as transfer girders in high-rise buildings, water tanks, pile caps, foundation walls, floor diaphragms, folded plate roof structures, shear walls or corbels. They have width that is small compared to their depth or span length and they basically loaded in their plane [2, 3]. Because of the small value of span to effective depth ratio، the strength of deep beams is usually controlled by shear rather than flexural strength. The internal stresses cannot be determined by ordinary beam theory and the common design procedures even in the elastic range. The strain or stress distribution along the depth of the deep beams is no longer a straight line, and the variation of the strains is dependent mainly on the shear span to depth ratio [4].In deep beams, unlike the slender one, the assumption that plane section before bending remains plane after bending is no longer applicable.

Shear strength of deep beams may be as much as two to three times greater than that calculated by using the ordinary equations which are used for the slender beams [5]. The most effective way to improve the shear strength of deteriorated deep beams is that externally bond FRP composite materials in the form of complete warps, U-jackets and side strips [6]. The use of carbon fiber composite material (FRP) in civil engineering for the strengthening or repairing of reinforced concrete structures and also for new constructions has become widespread practice. This strengthening system has several advantages like: high stiffness to weight ratio, corrosion resistance, improved durability and available in long lengths, flexibility in its use over steel plates, low thermal

expansion coefficient, rapid execution on site, high elastic modulus, high dynamic strength and no need for special equipment [7, 8].

This work is aims to using ANSYS computer program (version 15) to analyze seven lightweight aggregate deep beams made by the locally available porcelanite lightweight rocks and to present a numerical comparative study concerning the behavior of lightweight aggregate reinforced concrete deep beams strengthened by various orientations of CFRP strips. Shear response, load-deflection curves and crack patterns were elaborated. The model uses a smeared cracking approach.

2. Specimens Details

2.1 *Properties of Materials and Specimens Configuration*

All the seven lightweight aggregate concrete deep beams are having a rectangular cross section of (150 mm wide * 400 mm deep), with an overall length of (1400 mm). The effective depth is (350 mm). The adopted a/d ratios were (0.8, and 1.0) which satisfied the definition of the ACI 318M-2014 [1] Building Code for deep beam (a/d less than 2). The geometry, dimensions and the steel reinforcement details of the deep beams are given in Fig. 2. 3Φ16 mm and Φ5 @100 mm steel reinforcement bars were used for the main and shear reinforcement (in the vertical and horizontal directions) respectively, Table 1 gives the properties of the reinforcing bars used in this work.

Table 1: The properties of used steel reinforcing bars.

Reinforcing bar	Elastic modulus GPa	Bar Dia. (mm)	Yield stress (f_y) MPa	Ultimate strength (f_u) MPa	Elongation %
Main reinforcement	200	16	573	695	15.8
Shear reinforcement	200	5	476	578	4.61

From Table 1 above, the steel bars test results are complying with the ASTM A1064-14[9] and ASTM A615-05[10]. Steel ratio was equal to (ρs=0.01148) which is close to (ρmax =0.0125) per ACI 318M-2014 [1] for avoiding flexural failure so that the failure is governed by shear.

As recommended by ACI 213.2R-03 Committee [11], a concrete shall be deemed to be a structural lightweight concrete if its compressive strength is greater than (17 MPa) at 28 days and the oven dry density less than (2000kg/m^3). Hence, several trial mixes were made in order to satisfy these two conditions and reach to an acceptable concrete compressive strength of 26.34 MPa at 28 days with an oven dry density of about 1950 kg/m^3.

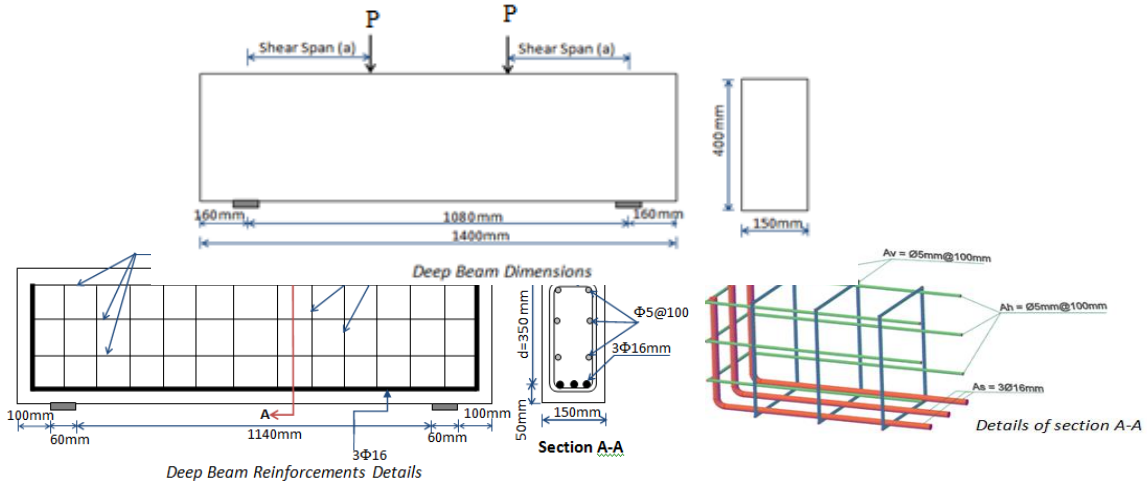

Figure 2.Deep beam geometry and reinforcement details

2.2 *Strengthening Configuration*

Five of the seven deep beams were strengthened by using carbon fiber strips in vertical, horizontal and inclined strips, the width and the thickness of theses strips were kept constant of 50 mm and 0.166 mm respectively. Table 2 gives the details of the specimens considered in this numerical investigation.

Table 2: Details of the deep beams specimens considered in this numerical investigation.

Beam designation	a/d	Beam Type	Shea reinforcement		No. of CFRP layers and orientation
			Shear reinforcement	CFRP Strips	
DB2	1.0	Control	Φ5 @ 100mm	none	-
DB4		wrapped	Φ5 @ 100mm	U-wrap	one layer/vertical
DB5		wrapped	Φ5 @ 100mm	horizontal wrapping	one layer/ horizontal
DB7		wrapped	Φ5 @ 100mm	Inclined	one layer/inclined
DB8		wrapped	Φ5 @ 100mm	U-wrap	two layer/vertical
DB11	0.8	Control	Φ5 @ 100mm	none	-
DB12		wrapped	Φ5 @ 100mm	U-wrap	one layer/vertical

DB4, DB8, and DB12 were strengthened by vertical CFRP strips as a U-shaped configuration as could be seen in Fig. 3a. These strips were spaced at 100mm c/c, knowing that DB8 was strengthened with double layers of CFRP strips. DB5 was strengthened by three longitudinal strips oriented horizontally with 100mm c/c spacing (Fig. 3b). In DB7, four isolated carbon fiber strips of 300mm and 200mm in lengths were bonded perpendicular to the diagonal connecting the loading and the supports points in a symmetrical manner with the 400 mm strip at the middle as shown in Fig. 3c. Decreasing in the strips length was adapted to be analogous to a decrease in the bottle shape representation of the strut and tie region (the load path). The Young's modulus and tensile strength of the used CFRP strips was of 330 GPa and 3.9 GPa respectively [12].

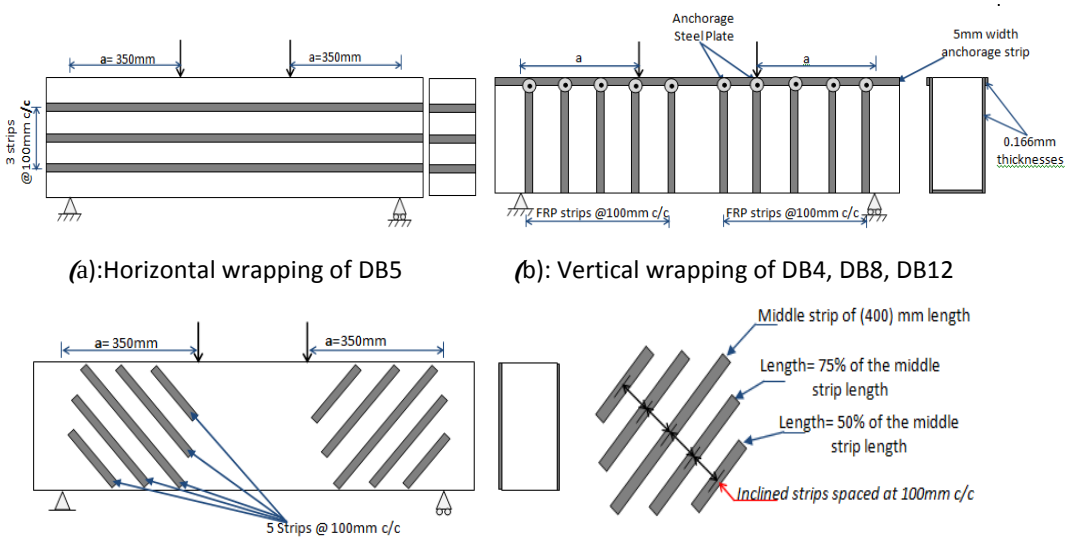

Figure 3. The CFRP wrapping Configuration

3. Ansys Finite Element Modeling

This paragraph will outline finite element analytical details for the shear deficient lightweight aggregate concrete deep beams after being strengthened with externally bonded CFRP strips. The widespread well-known ANSYS (version15) program is used for this purpose.

3.1 Material Modeling

3.1.1 Compressive Behavior of Concrete

In ANSYS, Drucker–Prager yield criterion was used to define the stress-strain behavior of the lightweight concrete. This curve is described by a piecewise linear stress-strain model. The uniaxial compressive stress-strain curve for the concrete was constructing by using (1) and (2) which were adopted by Desayi and Krishnan [13], along with (3) adopted by Gere and Timoshenko [14].

$$f = (E_c\,\varepsilon)/\left(1+\left(\frac{\varepsilon}{\varepsilon_\circ}\right)^2\right), \quad \varepsilon_1 \le \varepsilon \le \varepsilon_0 \tag{1}$$

$$\varepsilon_\circ = \frac{2f'_c}{E_c} \tag{2}$$

$$f = \varepsilon E_c \qquad 0 \le \varepsilon \le 0.3f'_c \tag{3}$$

$$f = f'_c \qquad \varepsilon_0 \le \varepsilon \le \varepsilon_{cu}$$

$$\varepsilon_1 = \text{the strain corresponding } to\ 0.3f'_c = 0.3f'_c/E_c$$

Here; f is the stress at a strain ε (MPa), ε_0 = strain at the ultimate compressive strength f'_c. The value of modulus of elasticity of concrete (E_c) in the present study was taken

from experimental results as 17850.06 MPa. The multilinear stress-strain diagram for concrete could be seen in Fig. 4.

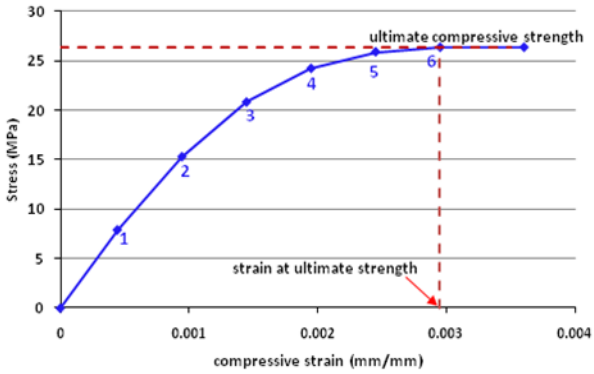

Figure 4: Uniaxial stress-strain relationship for the lightweight concrete

3.1.2 Steel Reinforcement Modeling

Elastic-perfectly plastic behavior is assumed to the steel reinforcement bars used in the present study. This behavior is identical in compression and tension. This model required the values of the steel modulus of elasticity, yield stress (fy) and the Poisson's ratio to be defined. The adopted elastic bilinear stress-strain curve of the reinforcing steel is shown in Fig. 5.

3.1.3 Frp Composites Modeling

Linear elastic properties for the CFRP strips were assumed as could be seen in Fig.6. The local coordinate system for the CFRP solid elements which was represented by shell 41 finite element is defined where the y-direction is the same as the fiber direction, and the x- and z-directions are perpendicular to the y-direction.

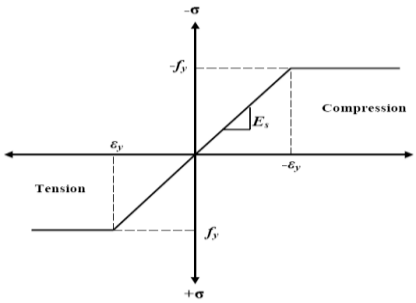

Figure 5: Stress-strain curve for steel reinforcement [15].

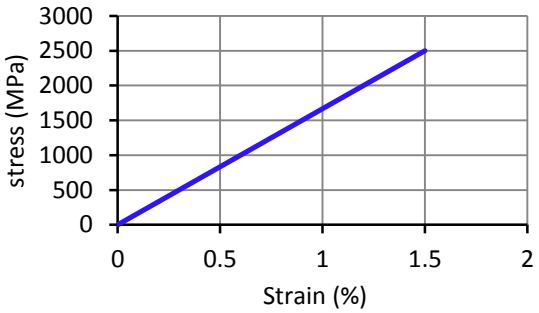

Figure 6: Linear Stress-strain curve for CFRP composite in the direction of the fiber.

3.2. Elements for Meshing

Lightweight aggregate concrete was modeled using Solid65 element. This element is a 3D structural reinforced concrete solid element. It has eight nodes with three degrees

of freedom per node; Solid65 can translate in the nodal x-, y- and z-directions. This element has the ability of plastic deformation, crushing and cracking in three orthogonal directions (*Fig.* 7a). Steel bars were modeled by using Link180 element for both the main and shear reinforcement in vertical and horizontal directions. It is a 3D spar element having two nodes with three degrees of freedom which were identical to those for solid65 and also this element has the capacity of plastic deformation (*Fig.* 7b). The bond between the concrete and the reinforcing bars is assumed to be perfect so the two materials shared the same nodes; the same approach was adopted for the bond between CFRP composite with the concrete.

In the finite element models as well as in the actual beams, four bearing steel plates were provided at the two points of loading and supports to avoids stress concentration and to prevent bearing failure of concrete at these zones. Solid185 finite elements were used to simulate the loading and supports steel bearing plates. It has eight nodes and three degrees of freedom per each node; translation in the nodal x-, y- and z- directions (*Fig.*7c).

The CFRP fabric strips were modeled using shell 41 element. This element is a 3D element with four nodes and three degrees of freedom per node; shell 41 can translate in the nodal x, y, and z directions (*Fig.* 7d).

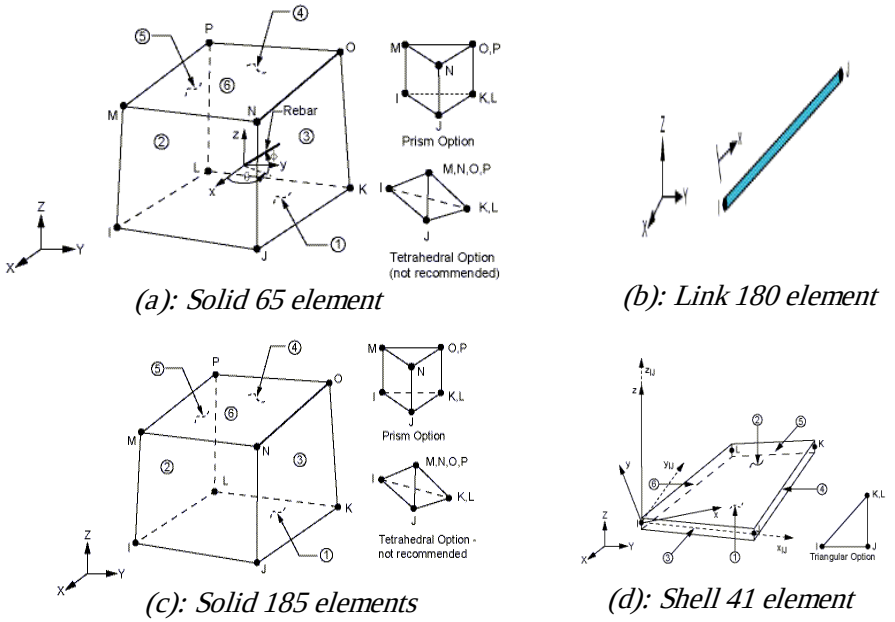

(a): Solid 65 element *(b): Link 180 element*

(c): Solid 185 elements *(d): Shell 41 element*

Figure 7: types of elements used in the present study [16].

3.3. Real Constants

Table 3 presents the real constants for the present model. Real Constant Set 1 is used for the Solid65 element in which, no real constant set exists for the element. In this work, modeling is bases on discrete reinforcement, and then zero values were entered for all real constants which switch off the smeared reinforcement capability of the Solid65 element. Values for cross-sectional area and initial strain were entered for the

Link180 element which was used to represent the steel reinforcement. No real constant was set for the solid 185 element which was used for bearing plates.

Table3: Real constant values.

Real constant set	Element	Description	Parameter	Value		
				Real constant for rebar		
				rebar 1	rebar 2	rebar 3
1	Solid65	Concrete	Material No.	0	0	0
			Volume ratio	0	0	0
			Orientation angle	0	0	0
			Orientation angle	0	0	0
2	Link 180	Main steel bars (3Φ16mm)	Cross sectional area (mm^2)	201.06		
			Initial strain (mm/mm)	0		
3	Link 180	Shear reinforcement (V and H)	Cross sectional area (mm^2)	19.635		
			Initial strain	0		
5	Shell 41	Carbon fiber	Shell thickness at node I TK(I)	0.166		
			node J TK(J)	0.166		
			node K TK(K)	0.166		
			node L TK(L)	0.166		

3.4. Material Properties

Table 4 illustrates the parameters needed to define the properties of the material used in the present work.

Material model No. 1 refers to the Solid65 element. To exactly model the concrete, Solid65 element required linear isotropic and multilinear isotropic material properties. The value of Poisson's ratio (ν) was assumed to be 0.15. Compressive uniaxial stress-strain relationship for the concrete model was obtained as explained in the paragraph (3-1-1). The uniaxial cracking stress was based upon the modulus of rupture. This value was found to be 3.12MPa by the experimental work done by the researchers. The material properties of Link180 (used for all the reinforcement) was assumed to be bilinear isotropic. Poisson's ratio for the steel reinforcement of the in this study was 0.3.

3.5. Meshing (Finite Element Discretization*)*

The mesh was set up such that rectangular elements were created in order to obtain good results from Soild65 element. The beams were represented by eight elements along the height, fifty-six elements along the length, while six elements were taken along the width of the beam. The finite elements representation and the typical steel reinforcement for the deep beam modeling in the present work are illustrated in *Fig.*8. No mesh of the reinforcement is needed because individual elements were created in the modeling through the nodes created by the mesh of the concrete volume. The advantage of geometrical symmetry was not utilized in the beam modeling in the present work

To simulate the strengthening system, CFRP strips are connected to the concrete elements as shown in Fig. 9. Full interaction theory was adopted to simulate the relationship between CFRP elements and concrete elements so that there is no slip between them. Also, Full bond was assumed between all reinforcement types embedded in concrete.

Table4: Material properties used in the present numerical work

Material model No.	*Element type*	*Material properties*
1	Solid 65	*Linear Isotropic*: EX 17850.06; PRXY 0.2 *Multilinear Isotropic*: *Point* 1 (0.000443, 7.902); *Point* 2 (0.000944, 15.291); *Point* 3 (0.001446, 20.811); *Point* 4 (0.001947, 24.208); *Point* 5 (0.00245, 25.879); *Point* 6 (0.00295, 26.340) Concrete: *ShrCf-Op* 0.1; *ShrCf-Cl* 0.7; *UnTensSt* 3.12; *UnCompSt* 26.34; *BiCompSt* 0; *HydroPrs* 0; *UnTensSt* 0; *TenCrFac* 0
2	Solid 185	*Linear Isotropic*: EX 200000; PRXY 0.3
3	Link 180	*Linear Isotropic*: EX 200000; PRXY 0.3 *Bilinear Isotropic*: Yield stress 573; *Tang Mod* 0
4	Link 180	*Linear Isotropic*: EX 200000; PRXY 0.3 *Bilinear Isotropic*: Yield stress 476; *Tang Mod* 0
5	Shell 41	Linear isotropic: Elastic modulus E 230000; Poisson's ratio PRXY .25; Shear modulus G_{xy} 94262.29

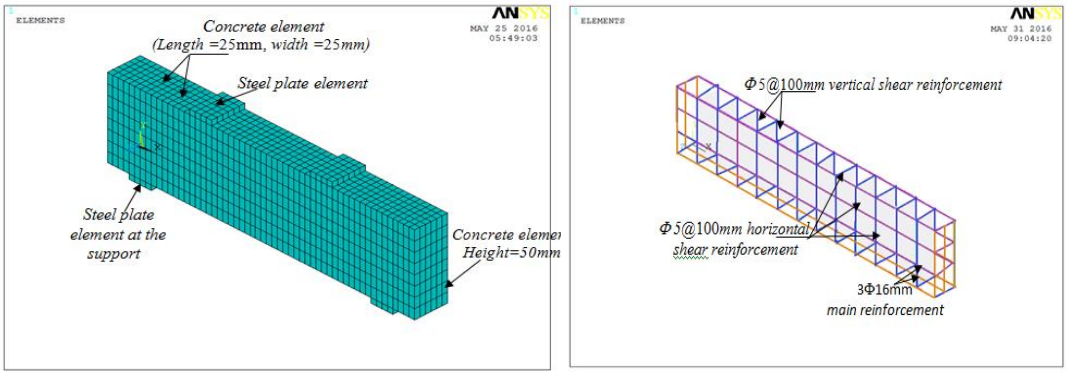

Figure 8: Finite element model and steel reinforcement representation for the analyzed deep beams

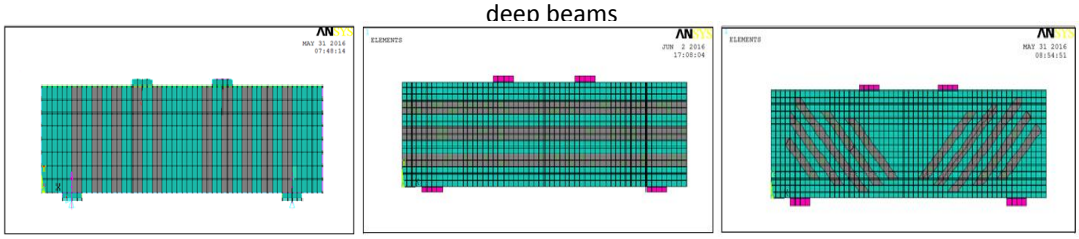

Figure 9: FRP layered solid elements configuration on the external surface of the deep beam

3.6. Loading and Boundary Conditions

Numerical model for the deep beams along with boundary conditions is shown in figure.10. To simulate the hinge support of the deep beam, single lines of nodes on the plate were given constraint in the UY, and UX directions and to simulate the roller support, the DOF in the UY was constraint. The load was applied to the load steel plate across the entire centerline in such a way that the concentrated force at each mid nodes on the centerline is (1/6) of the actual applied force and for the edge two nodes was (1/12) of the actual applied force as could be seen in figure 10.

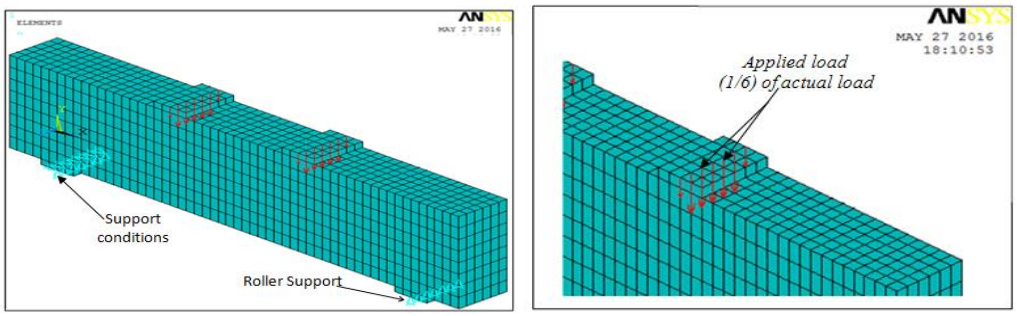

Figure 10: Applied loads and boundary conditions of the deep beams

3.7. Nonlinear Solution

Newton-Raphson approach was employs to solve the nonlinear equation in ANSYS computer program. In this approach, the total applied load is subdivided into a series of load steps. Newton-Raphson equilibrium iterations supply convergence at the end of each load increment within tolerance limits. The convergence tolerance limit was 0.005 for displacement checking in order to obtain convergence of the solutions.

4. Results and Discussion

4.1 First Crack Load and Ultimate Load Capacity

The results of the comparative verification study are presented in Table 5 for the first shear crack loads of the experimental tested deep beams $(P_{cr})_{Exp}$. with its corresponding results from the numerical analysis by using ANSYS, $(P_{cr})_{FEM}$. The ultimate loads results of the experimental work $(P_u)_{Exp}$, together with the final loads from the finite element models $(P_u)_{FEM}$. are also given in Table 5. The results are clear enough to reflect the acceptable conformity between the analytical and experimental data. In general, the first cracking load for the finite element analysis is somewhat higher than the experimental work. As an example, the first crack load of the control deep beam DB2 was 108.863 kN, which is about 9% higher than that of the experimental ones. The final loads for the finite element models are the last applied load steps before the solution begin to diverge due to numerous cracks and large deflections. The percentage difference for all the analyzed deep beams in case of first crack load was less than 19 %. The maximum deviation between the numerical and experimental results for the

ultimate load was about 15 %. Results of the Table 5 are also presented by bar charts as shown in Fig. 11 and Fig.12 for more illustration.

Table 5: Comparison between the experimental results and finite element analysis results

Deep Beam No.	a/d	First crack load (kN)		% difference	Ultimate load (kN)		(% difference	$(P_{cr})_{FEM}$ / $(P_u)_{FEM}$. %
		$(P_{cr})_{FEM}$	$(P_{cr})_{Exp}$		$(P_u)_{FEM}$	$(P_u)_{Exp}$		
DB2	1.0	108.86	100	9	435.45	440	1.03	25
DB4		171.60	160	7	484.67	520	6.79	35
DB5		106.95	120	10	465	500	7.00	23
DB7		161.92	140	16	578.3	580	0.29	28
DB8		96.93	120	19	520	560	7.14	19
DB11	0.8	94.39	100	6	524.36	620	15.43	18
DB12		163.59	170	4	605.88	680	10.90	27

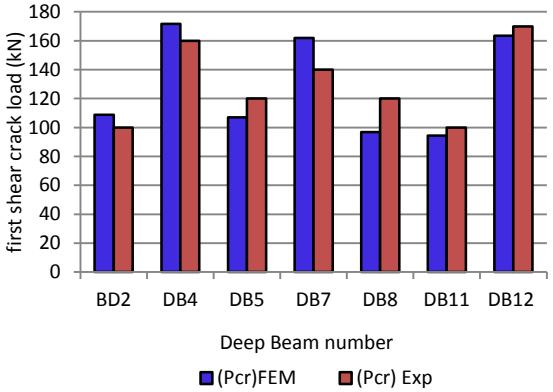

Figure 11: comparative verification study for the first shear crack loads of the experimental and numerical results

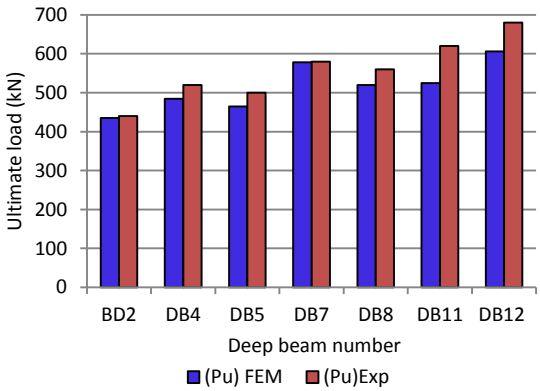

Figure 12: comparative verification study for ultimate loads of the experimental and numerical results

4.2 Load-Midspan Deflection behavior

The load-deflection curves of the numerical model compared with the experimental values for the unstrenghtened control deep beams (DB2 and DB11) and CFRP strengthened beams (DB4, DB5, DB7, DB8, and DB12) are shown in figure 13. Knowing that the experimental work was carried out by the researchers in the structural engineering laboratory/Building and Construction Engineering Department/ University of Technology. The strengthening details of these deep beams are given in Table 2. The deflections were measured at midspan length in the center of the bottom face of the deep beams. The curves showed clearly the acceptable agreement between the finite element and the experimental results throughout the entire range of behavior. In general, the finite element model of the analyzed deep beams were stiffer in behavior compared with the actual beams, that may be clarified as; perfect bond between the concrete elements and the reinforcement is assumed in the ANSYS analysis, but for the actual beams the assumption would not be true because the slip may occurs. Therefore, in the actual beams, the composite action between the steel reinforcing and concrete is lost. In addition to that, the presence of the microcracks (which is generated by drying

shrinkage and handling) would reduce the stiffness of the actual beams, while the finite element models do not include such cracks as result to factors that are not incorporated into the models.

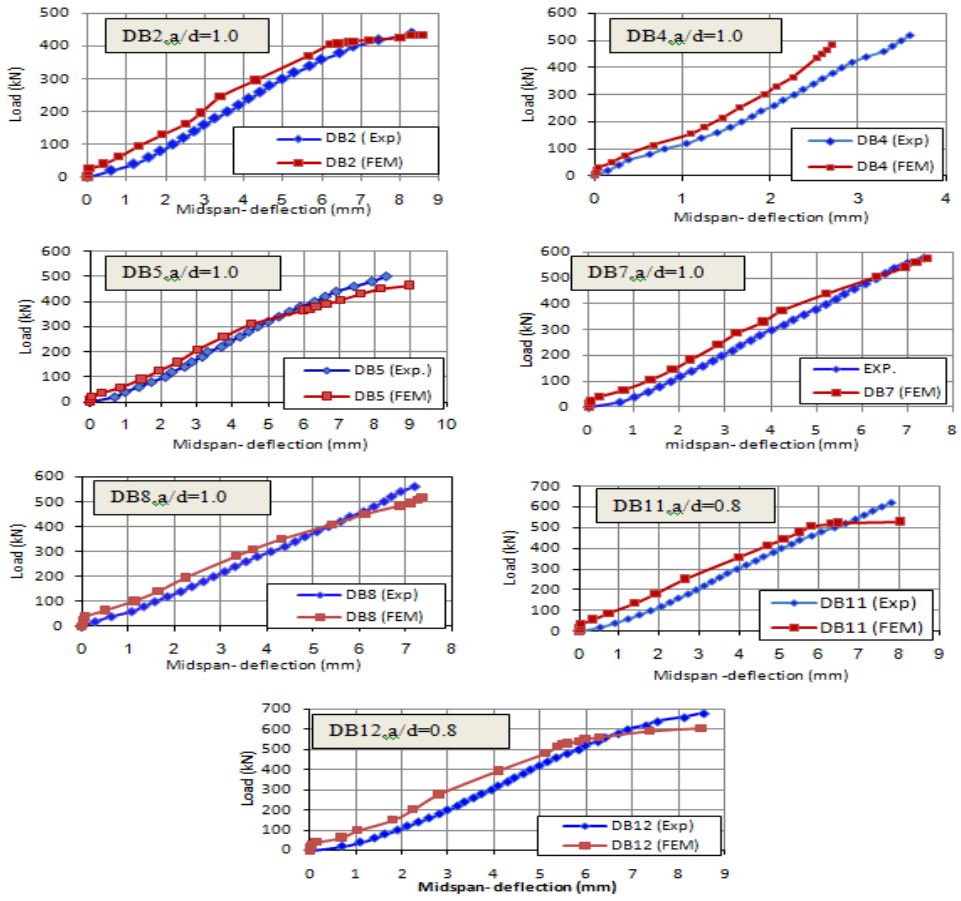

Table 6 illustrates the comparison between the midspan deflection of the experimental tested deep beams, $(\delta_v)_{Exp.}$ measured at ultimate load and the maximum midspan deflection from the finite element models $(\delta_v)_{FEM.}$ it can be concluded from this table that the finite element analysis agrees well with the experimental results.

Table 6: Comparison between the experimental and finite element results of deflections for the deep beams at ultimate load.

Deep Beam No.	a/d	Deflection (mm) $(\delta_v)_{Exp.}$	Deflection (mm) $(\delta_v)_{FEM.}$	$(\delta_v)_{FEM}$ / $(\delta_v)_{Exp.}$
DB2	1	8.3	8.57	1.03
DB4		3.6	2.59	0.72
DB5		8.3	8.95	1.08
DB7		7.35	7.31	0.995
DB8		7.2	7.36	1.02
DB11	0.8	7.6	8.02	1.06
DB12		8.54	8.49	0.994

4.3. *Crack Pattern*

The crack patterns obtained by ANSYS program at failure load for the tested deep beams are shown Fig.14 to 20. The crack pattern in DB2 (which is the control beams with a/d =1) is distributed in a large area within the strut path zone. At the load of (108.863 kN) first crack appeared. Later with the increase in loading values the crack propagated further. DB2 failed completely in shear showing frame type failure. The deflections obtained using ANSYS are in good agreement when compared with experimental results. It is noticed from the crack pattern figures that many adjoining diagonal cracks extend from the loading point towards the bottom nodes and crushing of concrete occurs below the loading plate. These cracks are simulating the bottle shape of the strut zone and they are in good agreement with the mode of failure obtained in the experimental work.

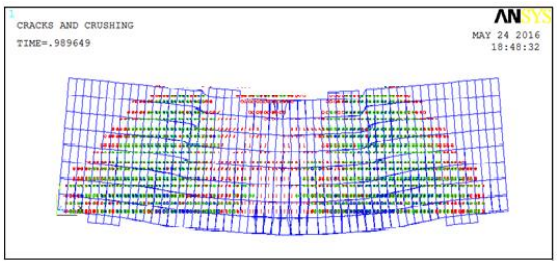

Figure 14: crack pattern of unstrenghtened control deep beam DB2, a/d=1.0

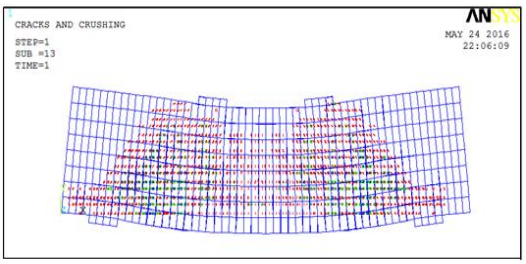

Figure15: crack pattern of DB4 strengthened by one layers vertical CFRP strips, a/d=1.0

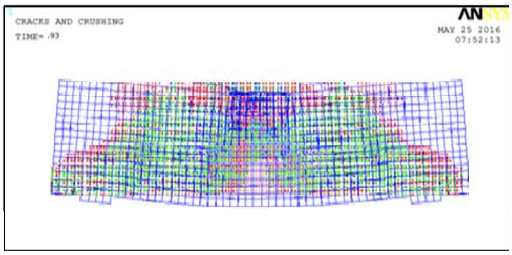

Figure 16: crack pattern of DB5 strengthened by one layer horizontal CFRP strips, a/d=1.0

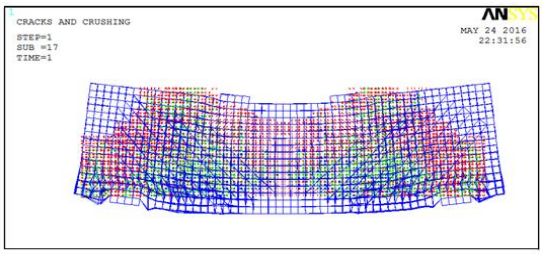

Figure 17: crack pattern of DB7 strengthened by one layer inclined CFRP strips, a/d=1.0

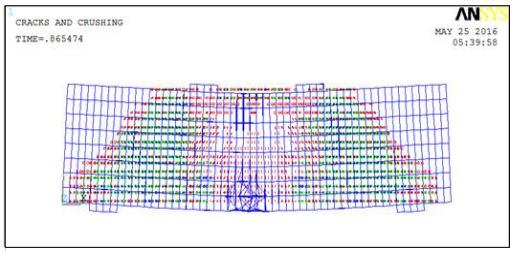

Figure 18: crack pattern of unstrenghtened control deep beam DB8, a/d=0.8

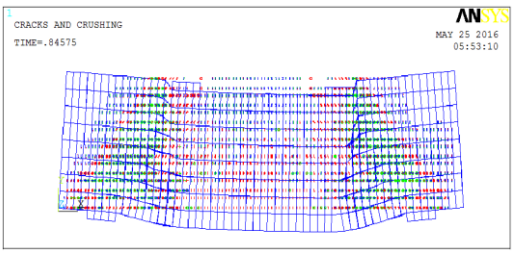

Figure 19: crack pattern of unstrenghtened control deep beam DB11, a/d=0.8

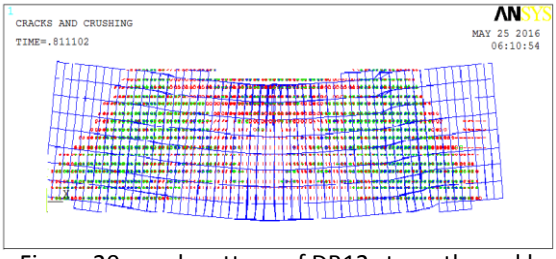

Figure 20: crack pattern of DB12 strengthened by one layer vertical CFRP strips, a/d=0.8

5. Summary and Conclusions

Although the number of tested deep beams was limited, a consistent tendency in their response is observed. Nonetheless, further experimental and numerical research may be needed to confirm the reproducibility of this study. Based on the numerical and experimental results discussed in this paper, the following conclusion are drawn

1- The general behavior of the finite element model shows a reasonable agreement with the experimental data obtained in this work on the same deep beams in the same geometry, internal steel and material properties. The added CFRP external strips to the deep beams improved the behavior and load carrying capacity of the strengthened deep beams compared the control ones.

2- The slight difference between the experimental and numerical results indicates that the finite element models assumptions of full interaction between the CFRP strips and concrete was reasonable.

3- The failure mechanism of the tested lightweight reinforced concrete deep beams is modeled quite well using ANSYS software. The failure load measured as well as overall behavior of the analyzed deep beams was close to the experimental results.

4- Bonded CFRP system in the shear span considerably delayed the formation of diagonal shear cracks and provided positive restraint to the subsequent growth of cracks. Furthermore, more distribution and smaller crack amplitude were detected at mid depth within the shear span of the strengthened beams with respect to the control deep beams.

5- It is verified that the finite element analysis can accurately predict the load-deformation, load capacity and failure mode of the deep beam. It can also capture cracking process for the shear-flexural peeling and end peeling failures, similar to the experiment.

Acknowledgement

The authors may express their appreciation to relevant agencies and related personnel providing academic advice to their research.

6. References

1. ACI Committee 318, " Building Code Requirements for Structural Concrete (ACI 318M-14) and Commentary on Building Code Requirements for Structural Concrete (ACI 318R-14)," American Concrete Institute, Farmington Hill, 2014, 524pp.
2. Russo, G.; Venir, R.; and Pauletta, M., "Reinforced Concrete Deep Beams-Shear Strength Model and Design Formula," ACI Structural Journal, Vol. 102, No. 3, May-June, 2005, pp.429-437.
3. Nagarajan, P; Pillai, T.M.M.; and Ganesan, N., (2007)." Design of Simply Supported Deep Beams Using IS 456:2000 and Strut and Tie Method," IE (I) Journal-CV, Vol.88, pp. 38-43.

4. Niranjan, B.R.; and Patil, S.S. (2012). " Analysis of R.C Deep Beam by Finite Element Method ," International Journal of Modern Engineering Research (IJMER), Vol. 2, No. 6, pp.4664-4667
5. Sveinsdottir, S.L. (2012) "Experimental Research on Strengthening of Concrete Beams by the Use of Epoxy Adhesive and Cement-Based Bonding Material," MSc thesis, Reykjavik University, School of Science and Engineering, Iceland, 125pp.
6. Chen, G.M; Teng, J.G.; and Chen, J.F., (2013), "Shear Strength Model for FRP-Strengthened RC Beams with Adverse FRP-Steel Interaction," Journal of Composites for Construction, ASCE, Vol.17, No.1, pp.50-66.
7. Alferjani, M.B.S.; Abdul Samad, A.; and Elrawaff, B.S. (2014). "Shear strengthening of reinforced concrete beams using carbon fiber reinforced polymer laminate: A review", American Journal of Civil Engineering, Vol.2, No.1, pp 1-7.
8. Dolan, C.W.; Hamilton, H.R.; and Nanni, A. (2001). "Design Recommendations for Concrete Structures Prestressed with FRP Tendons," Final Report, FHWA Contract, Vol. 1, 133pp.
9. ASTM A1064/A1064N-14, (2014), "Standard Specifications for Carbon-Steel Wires and Welded Wire Reinforcement, Plain and Deformed, for Concrete ," ASTM Subcommittee A01.05 on Steel, Stainless Steel, and Related Alloys, Vol.01.04, West Conshohocken, A, USA, Published in November, 5pp.
10. ASTM A615/A615M-16, "Standard Specifications for Deformed and Plane Carbon-Steel Bars for Concrete Reinforcement," ASTM Subcommittee A01.05 on Steel, Stainless Steel, and Related Alloys, Vol. 01.04, West Conshohocken, A, USA, , Published in March 2016, 8pp.
11. ACI Committee 213.2R-03. (2003). "Guide for Structural Lightweight- Aggregate Concrete," American Concrete Institute, Farmington Hill, USA, 38pp.
12. Sika warp-300 C/60. "Woven Carbon Fiber Fabric for Structural Strengthening," Revision No: 1, Identification No, 01 04 01 02 001 0 000011, Istanbul, Turkey, Product Data Sheet, Edition 24/08/2009.
13. Desayi, P.; and Krishnan, S. (1964). "Equation for the Stress-Strain Curves of Concrete," ACI Journal, Vol. 61, No. 3, pp. 345-350.
14. Gere, J.M.; and Timoshenko, S.P. (1997). "Mechanics of Materials," 4th edition, Boston, Massachusetts, ,
15. Kachlakev, D.; Miller, T.; and Yim, S. (2001). "Finite Element Modeling of Reinforced Concrete Structures strengthened With FRP Laminates," Final Report, Oregon Department of Transportation, Research Group and Federal Highway Administration, Washington, DC 20590, pp. 113.
16. ANSYS-Release Version 15.0, " ANSYS Help,", Copyright 2015